Cavity-configuration-dependent nonlinear dynamics in Kerr-lens mode-locked lasers

Ming-Dar Wei and Wen-Feng Hsieh

Institute of Electro-Optical Engineering, National Chiao-Tung University, Ta-Hsueh Road 1001, Hsinchu 30050, Taiwan

Received November 15, 1999; revised manuscript received March 16, 2000

We determined theoretically that the nonlinear dynamics of a Gaussian beam is configuration dependent in a general cavity. This prediction was confirmed by numerical simulation in a Kerr-lens mode-locked cavity for which the self-focusing effect is considered the nonlinear source in both the spatial and the temporal domains. Period doubling, tripling, and quadrupling can occur in these configurations with the products of generalized cavity G parameters equal to 1/2, 1/4 (or 3/4), and $(2 \pm \sqrt{2})/4$, respectively. The dynamic behavior of the cavity beam will become irregular if the nonlinear effect is further increased. © 2000 Optical Society of America [S0740-3224(00)00708-6]

OCIS codes: 140.3410, 140.4050, 260.5950, 140.1540.

1. INTRODUCTION

The nonlinear Kerr effect can induce not only Kerr-lens mode locking but also fruitful nonlinear dynamics. After the discovery of Kerr-lens mode locking in Ti:sapphire lasers,[1] various theoretical studies were dedicated to the Kerr-lens mode-locked (KLM) cavity design, both numerically and analytically.[2–6] Among these theoretical studies, most efforts were concentrated on the mode-locking mechanisms that result from self-amplitude modulation, which originates from the power-dependent cavity beam's being modified by the self-focusing effect inside the Kerr medium. Because a femtosecond pulse will simultaneously undergo self-amplitude and self-phase modulation as it propagates through a Kerr medium, coupling of spatial and temporal effects results from the Kerr nonlinearity. One may model this problem by preserving the total pulse energy at that moment.[7,8] In fact, the analyses that considered self-amplitude modulation only in the spatial domain agree with the experimental results and offer valuable suggestions for KLM cavity designs.

Reports of nonlinear dynamic studies of KLM lasers, however, are somewhat limited. Recently, period doubling of a Ti:sapphire laser was observed near the edge of a stable region and was explained in terms of total mode locking[9]; the simultaneous locking of the TEM_{00} and the TEM_{01} modes results in spatial sweeping of the beam with a frequency determined by the spacing between these two modes. A detailed study of subharmonic oscillations by total mode locking was reported in Ref. 10. Besides the dynamics that involves the phase locking of both transverse and longitudinal modes, the dynamic behavior based on the propagation of a single Gaussian beam, including self-focusing and loss effects,[11] was numerically investigated. By use of geometric (spot size and curvature) and energetic (gain and intensity) variables in a KLM system, regular, quasi-periodic, and chaotic behaviors were obtained in a KLM laser whose configuration was close to the limit of the stable region. These theoretical predictions were supported by the observation of quasi-periodic and chaotic behavior in a ring Ti:sapphire laser with an equivalent Fabry–Perot configuration.[12] Apparently, single-Gaussian-mode propagation reveals complicated dynamics in KLM cavities.

According to a previous theoretical study[13] and the prediction of Greene's residue theorem,[14] some specific cavity configurations within the geometrically stable region of a cold cavity[15] will be highly sensitive to the nonlinear effect. On the basis of this theoretical prediction, in this paper we present the cavity-configuration-dependent dynamic behavior of KLM lasers by modeling the nonlinear dynamics of single-Gaussian mode propagation in a KLM cavity. The dynamics is directly induced by self-focusing even with a single Gaussian mode and is different from that of that total mode locking that consists of both transverse and longitudinal modes. The propagation of a Gaussian beam in the spatial domain is governed by the *ABCD* law in linear elements[15,16] and is solved by the renormalized q-parameter method in the Kerr medium.[17] We neglect the thermal lens effect because it may simply shift the cavity configuration and play a minor role in the ultrashort-pulse dynamics.[11] Our numerical results confirm the theoretical prediction that the multiple periods of pulse trains in a KLM cavity depend on the cavity configuration, even if spatial–temporal coupling is considered. The evolution of the system will become irregular if the nonlinear effect is further increased.

This paper is organized as follows: In Section 2 we apply Greene's residue theorem to discuss the stability of a general lossless cavity and find new specific cavity configurations that may become unstable in the presence of a persistent nonlinear effect. A numerical simulation of the nonlinear dynamic behavior of a KLM cavity in the spatial domain is described in Section 3. The results of combining the spatial and the temporal domains are presented in Section 4, and irregular evolution as the intra-

cavity intensity is increased is discussed in Section 5. In Section 6 we briefly discuss the difference between our approach and that of total mode locking. Finally, conclusions are drawn in Section 7.

2. STABILITY OF A GENERAL LOSSLESS CAVITY

Consider a Gaussian beam propagating on the ζ axis; we can write its complex field as[15]

$$u(r, \zeta) = \left[\frac{U}{w(\zeta)}\right]\exp\left[-i\frac{kr^2}{2q(\zeta)}\right], \tag{1}$$

with the complex beam parameter

$$\frac{1}{q(\zeta)} = \frac{1}{R(\zeta)} - i\frac{\lambda}{\pi w(\zeta)^2}, \tag{2}$$

where r is the radial distance from the ζ axis, U is the real amplitude, λ is the central wavelength, R is the phase-front radius of curvature, and w is the spot size of the beam. When the Gaussian beam propagates through optical components, the transformation of the q parameter obeys the so-called *ABCD* law that has been widely applied to designing stable laser cavities.[15,16] Assuming that the round-trip matrix of the cavity is $\begin{bmatrix} A & B \\ C & D \end{bmatrix}$, the relationship of beam parameter of the $(n+1)$st round trip to that of the nth round trip can be written as

$$w_{n+1} = f_w(w_n, R_n) = \left\{-\frac{\pi}{\lambda}\mathrm{Im}\left[\frac{C + D(1/R_n - i\lambda/\pi w^2)}{A + B(1/R_n - i\lambda/\pi w^2)}\right]\right\}^{-1/2}, \tag{3}$$

$$R_{n+1} = f_R(w_n, R_n) = \left\{\mathrm{Re}\left[\frac{C + D(1/R_n - i\lambda/\pi w^2)}{A + B(1/R_n - i\lambda/\pi w^2)}\right]\right\}^{-1}, \tag{4}$$

where Re and Im stand for the real and the imaginary parts, respectively, of a complex number. Thus Eqs. (3) and (4) form a two-dimensional iterative map. If all the elements of the *ABCD* matrix are real, i.e., if the cavity is lossless, this map is a conservative one.[18] Inasmuch as the fixed point of the map is just the self-consistent solution of the cavity design, to determine the characteristics of the cavity beam one needs to discuss the stability of the fixed point.[18,19] It is convenient to study the stability of the conservative map by using Greene's residue theorem and to define the residue as[14]

$$\mathrm{Res} = [2 - \mathrm{Tr}(M_J)]/4, \tag{5}$$

where M_J is the Jacobian matrix of the map and $\mathrm{Tr}(M_J)$ is its trace. The relationship between the residue and the phase shift, θ, of the map per iteration can be represented as[14]

$$\mathrm{Res} = \sin^2(\theta/2). \tag{6}$$

From Eqs. (3)–(5), the residue of a lossless standing-wave cavity is[13]

$$\mathrm{Res} = 1 - (2G_1G_2 - 1)^2, \tag{7}$$

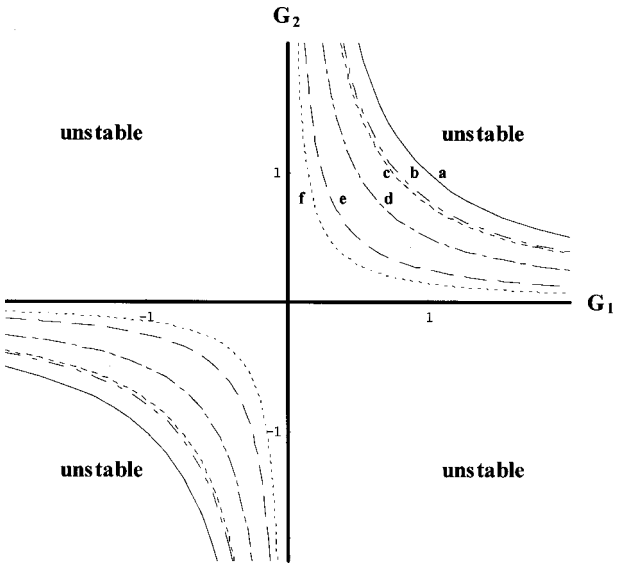

Fig. 1. Stability diagram for a general resonator. Besides the stable regions ($0 < G_1G_2 < 1$), the specific configurations are shown as a, $G_1G_2 = 1$; b, $G_1G_2 = (2+\sqrt{2})/4$; c, $G_1G_2 = 3/4$; d, $G_1G_2 = 1/2$; e, $G_1G_2 = 1/4$; f, $G_1G_2 = (2-\sqrt{2})/4$.

where $G_1 = a - b/\rho_1$ and $G_2 = d - b/\rho_2$ represent the G parameters of a general optical cavity, $\begin{bmatrix} a & b \\ c & d \end{bmatrix}$ is the transfer matrix of single pass between the two end mirrors, and ρ_1 and ρ_2 are the radii of curvature of the two end mirrors.

From the residue theorem, the fixed point is stable when $0 < \mathrm{Res} < 1$, whereas it is unstable when $\mathrm{Res} < 0$ or $\mathrm{Res} > 1$. With the help of Eq. (7), we found that the region with $0 < G_1G_2 < 1$ is stable and the regions with $G_1G_2 < 0$ and $G_1G_2 > 1$ are unstable. This result is the same as for the geometrically stable condition.[15] Besides the $\mathrm{Res} = 0$ and $\mathrm{Res} = 1$ being critical, the residue theorem proposes that the orbit is stable for $0 < \mathrm{Res} < 1$, except for $\mathrm{Res} = 3/4$ and $\mathrm{Res} = 1/2$ (sometimes). These special cases with $\mathrm{Res} = 0, 1, 3/4, 1/2$ correspond to the low-order resonances where $p = 1, 2, 3, 4$ in $\chi^p = 1$, respectively. Here χ is the eigenvalue of M_J. Under these circumstances, linearization of M_J at these fixed points is not sufficient to describe the behavior of the nearby points, and complicated dynamics may occur at these configurations if there is a persistent nonlinear effect. These special conditions correspond to $G_1G_2 = 0$ or $G_1G_2 = 1$ for $\mathrm{Res} = 0$ and $G_1G_2 = 1/2$ for $\mathrm{Res} = 1$, $G_1G_2 = 1/4, 3/4$ for $\mathrm{Res} = 3/4$, and $G_1G_2 = (2 \pm \sqrt{2})/4$ for $\mathrm{Res} = 1/2$. In Fig. 1 a diagram of the stable region is shown in which the dashed curves represent these special configurations. It is worth noting that these configurations are located within the geometrically stable regions, except that $G_1G_2 = 0,1$ is geometrically critically stable. Nonlinear effects may break the stability of a self-consistent Gaussian beam in these special configurations.

3. KERR-LENS MODE-LOCKED CAVITY

In a KLM cavity the nonlinear self-focusing effect within the Kerr medium modifies the profile of the cavity mode and leads to mode locking. The self-focusing effect may simultaneously induce complicated nonlinear dynamics of

the cavity beam as the effect further increases. Because the self-focusing effect dominates the characteristics of a KLM cavity, this accompanying nonlinear dynamics is worth considering, particularly for the specific configurations with low-order resonances.

Figure 2 shows a four-mirror KLM cavity with two arms, d_1(= 70 cm) and d_2(= 100 cm), a Brewster-cut Ti:sapphire rod of length L_c = 20 mm, and curved mirrors M_2 and M_3 with 100-mm radii of curvature. The curved mirrors are tilted by $\theta = 15.4°$ to compensate for the astigmatism of the Brewster-cut laser rod.[20] The analysis of the propagation of the Gaussian beam is divided into two parts; the *ABCD* law is applied for linear optical components and the renormalized q-parameter method[6,17] is used in the Kerr medium. From the renormalized q-parameter method we can transform the q parameter from end face I to end face II of the Kerr medium as

$$\frac{1}{q_{\mathrm{II}}} = \frac{1}{R_{\mathrm{II}}} - i\frac{\lambda}{\pi w_{\mathrm{II}}^2} = \frac{\left[\frac{1}{R_{\mathrm{I}}} + \frac{L}{R_{\mathrm{I}}} + L(1-K)\left(\frac{\lambda}{\pi w_{\mathrm{I}}^2}\right)^2\right] - i\left(\frac{\lambda}{\pi w_{\mathrm{I}}^2}\right)}{\left(1 + \frac{L}{R_{\mathrm{I}}}\right)^2 + L^2(1-K)\left(\frac{\lambda}{\pi w_{\mathrm{I}}^2}\right)^2}, \tag{8}$$

where $L = L_C/n_0$ is the effective length, n_0 is the index, and L_C is the physical length of the Kerr medium. The Kerr parameter K is defined as

$$K = \frac{8\pi n_2 P}{\lambda^2}, \tag{9}$$

where n_2 is the nonlinear refractive index and P is the intracavity peak power.

Let the reference plane be the place where the beam just leaves end mirror M_1. By cascading the propagation of q parameter in a round trip, the complicated transformation of the q parameter that relates the $(n+1)$st to the nth round trip forms a two-dimensional iterative map, similarly to the approach described in Section 2. The map is simply represented as

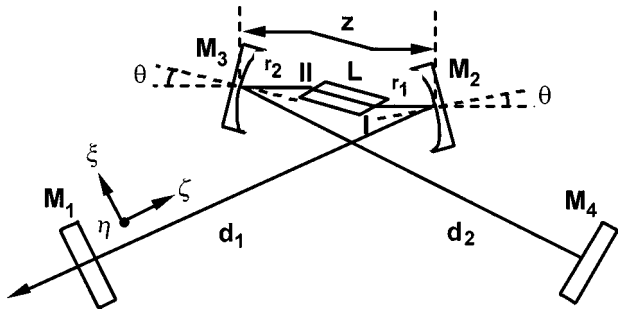

Fig. 2. Four-mirror KLM laser standing-wave resonator. A Kerr medium with length L is placed between curved mirrors M_2 and M_3 of high reflection. M_1 is the output coupler and M_4 are flat mirrors with high reflection.

Table 1. Configurations with Several z Values that Have Low-Order Resonances

Residue	G_1G_2	z (mm)	Dynamic Behavior
1/2	$(2-\sqrt{2})/4$	114.386	Period-4
		117.322	
	$(2+\sqrt{2})/4$	112.617	
		119.091	
3/4	1/4	114.017	Period-3
		117.691	
	3/4	112.811	
		118.897	
1	1/2	113.340	Period-2
		118.367	

$$w_{n+1} = f_w(w_n, R_n; K), \tag{10}$$

$$R_{n+1} = f_R(w_n, R_n; K). \tag{11}$$

We can label the map as

$$\mathbf{Q}_{n+1} = \mathbf{F}_K(\mathbf{Q}_n), \tag{12}$$

where $\mathbf{Q}_n = \left[\begin{smallmatrix} w_n \\ R_n \end{smallmatrix}\right]$ and n represents the number of iterations. Kerr parameter K corresponds to the nonlinear parameter in this map. From Eq. (8) we find that the map reduces to a linear cavity system as $K = 0$. The system with $K = 0$ represents a cw operation in the KLM cavity.[21] Increasing K results in nonlinearly modifying the cavity beam to induce mode locking, and the system is at pulse operation.

From the discussion in Section 2, the behavior of the cavity beam in cavity configurations with Res = 1/2, 3/4, 1 cannot be determined by linear stability analysis and may become complicated under the influence of the nonlinear effect. We numerically study the nonlinear behavior at these configurations. We constrain K to less than 0.4 in our numerical simulation because such a condition can be achieved in experiments. In fact, the steady-state K values are usually greater than 0.4 in the experimental results. For example, a 60-fs Ti:sapphire laser with 2-W average output power from a 21% output coupler as described in Ref. 22 corresponds to $K = 0.65$.

Because similar dynamic behavior occurs in the sagittal and the tangential planes, we concentrate our numerical simulations on the sagittal plane only. The two adjustable variables are z and r_1, where z is the separation of the two curved mirrors and r_1 is the distance between curved mirror M_2 and the rod end face I. The z value largely determines the geometrically stable region, and r_1 affects the efficiency of the Kerr effect. Table 1 lists the configurations and z values that correspond to low-order resonances at $K = 0$. Because there are two stable regions, each G_1G_2 will have two z values.

Considering the case with z = 113.34 mm, where the configuration is near $G_1G_2 = 1/2$, we found period-doubling bifurcation in the spot size when nonlinear parameter K increased. The period-2 fixed point, $\mathbf{Q}^{(2)}$, is the solution of $\mathbf{F}_K\{\mathbf{F}_K[\mathbf{Q}^{(2)}]\} - \mathbf{Q}^{(2)} = 0$. It is clear that the $\mathbf{Q}^{(2)}$ represents the self-consistent Gaussian beam of two round trips. Figure 3 is the bifurcation diagram at r_1 = 42 mm, which shows the relationship between the

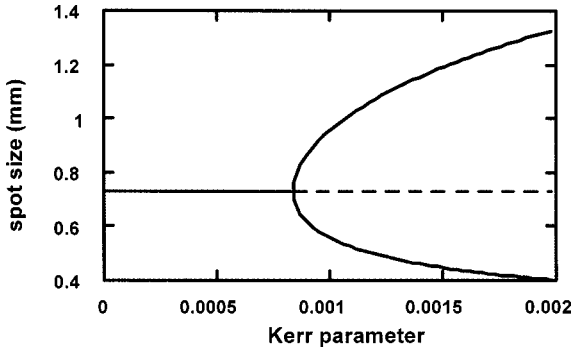

Fig. 3. Period-doubling bifurcation. As $K > K_c = 0.0008353$, the solid line of period-2 represents the stable pair of solutions that corresponds to the self-consistent Gaussian beam of two round trips. Period-1 is unstable (shown as a dashed line).

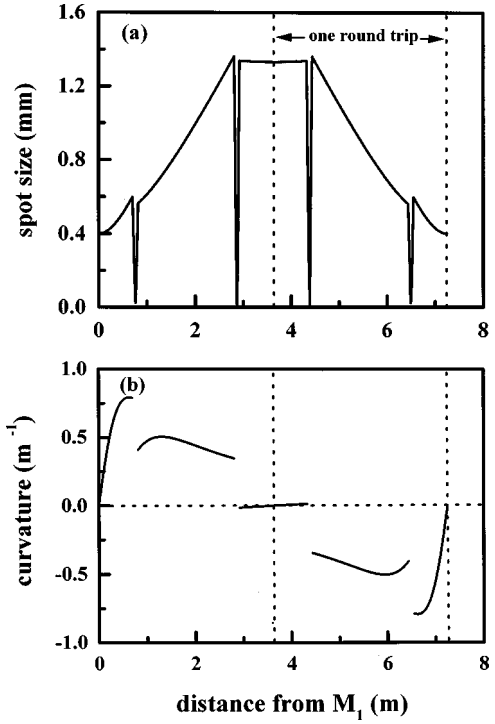

Fig. 4. Evolution of (a) spot size and (b) curvature for the period-2 solution. The two period-2 solutions, $(w, 1/R) = (0.40\,\text{mm}, 0)$ and $(w, 1/R) = (1.33\,\text{mm}, 0)$ with $z = 113.34\,\text{mm}$, $x = 42\,\text{mm}$, and $K = 0.002$, are the self-consistent Gaussian beam solutions of two round trips. The variation of curvature between the two curved mirrors is too large to be shown in this figure.

spot size and the Kerr parameter. This evolution belongs to the direct period-doubling bifurcation.[23] The critical value of K at which the transition to period-2 takes place approximates $K_c = 0.0008353$. There is only one stable period-1 solution as $K < K_c$; however, a pair of stable period-2 fixed points exists, and the period-1 fixed point becomes a separatrix in phase space as $K > K_c$.[23] We further choose a period-2 case to depict the propagation of cavity beam in two round trips. Figure 4 shows the spot size and curvature of a period-2 cavity beam along the cavity with $K = 0.002$. The two period-2 fixed points at M_1 are $(w, 1/R) = (0.40\,\text{mm}, 0)$ and $(w, 1/R) = (1.33\,\text{mm}, 0)$. We find that the spot size changes once for a round trip and repeats itself after two round trips, whereas the curvature of Gaussian beam always matches that of the end mirror for each round trip.

In fact, the Poincare–Birkhoff theorem tells us that some of period-2 fixed points survive if a nonlinear term is added to perturb the critical stable system with Res = 1.[24] Apparently, this theorem governs the simulation results that the configurations near $G_1G_2 = 1/2$ develop to period-2 under the influence of the nonlinear effect. Because self-focusing causes the equivalent configuration to change, the configuration near $G_1G_2 = 1/2$ can also cause a period-doubling bifurcation. A contour plot of K_c (with $K_c < 0.1$) as a function of z and r_1 is shown in Fig. 5. The region where period doubling exists is ~60 μm for z, and for other values of z it ranges from several to tens of millimeters for r_1. Moreover, the intracavity peak power required for reaching period doubling decreases and becomes smaller than that of the initial pulse buildup as the configuration approaches $G_1G_2 = 1/2$. From the experimental result of Ref. 25, the initial coherent spike of pulse buildup is approximately 10–40 ps as a result of partial phase locking of the longitudinal modes. The calculated K of the initial spike for 40 ps is ~0.001 in a KLM laser with an intracavity average power $P_{\text{av}} = 10\,\text{W}$ and a 100-MHz repetition rate. This K is slightly larger than some K_c, for example, the aforementioned $K_c = 0.0008353$ with $z = 113.34\,\text{mm}$ and $r_1 = 42\,\text{mm}$, which implies that a KLM laser operating at this configuration can directly build up a period-2 pulse train. Nevertheless, the region in which such a condition is satisfied is less than 1 μm for z, and K_c increases rapidly to greater than 0.01 when z is set 10 μm away from $G_1G_2 = 1/2$, as shown in Fig. 5. Thus, it may not be easy experimentally to observe period doubling before the build-up duration. However, most of the experiments with $K \geqslant 0.4$ are greater than those with K_c depicted in Fig. 5. Therefore we believe that period doubling can be observed at the configuration near $G_1G_2 = 1/2$, which is in the middle of the stable region.

When we alter the configuration to the nearby $G_1G_2 = 1/4$ (or $G_1G_2 = 3/4$), period-tripling bifurcation occurs. $G_1G_2 = 1/4$ (or $G_1G_2 = 3/4$) has Res = 3/4, which stands for the average angle of rotation per period, $\theta = 2\pi/3$,

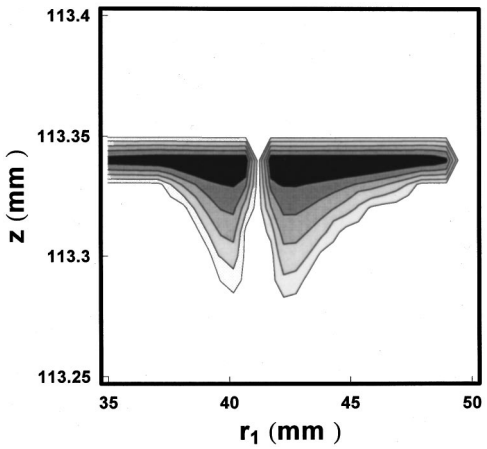

Fig. 5. Contours of the critical bifurcation parameter for period-2. The gray levels, from dark to light, correspond to $K_c = 0.02, 0.04, 0.06, 0.08, 0.1$.

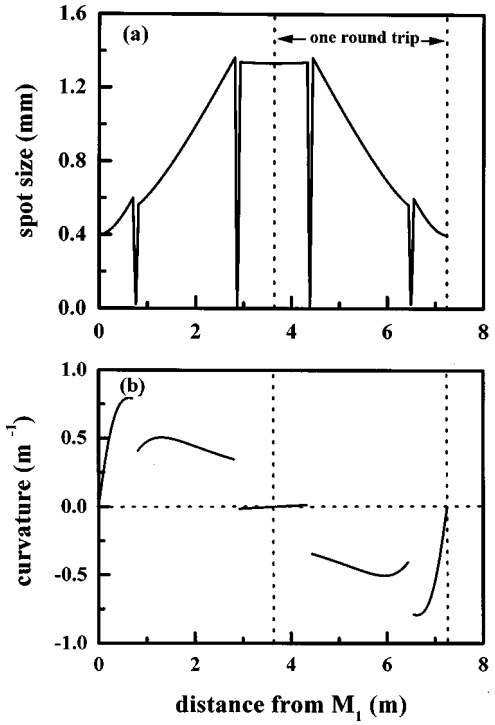

Fig. 6. Evolution of (a) spot size and (b) curvature for the period-3 solution. The period-3 solutions are $(w, 1/R) = (0.75\,\text{mm}, 0)$, $(w, 1/R) = (0.64\,\text{mm}, 0.14\,\text{m}^{-1})$, $(w, 1/R) = (0.64\,\text{mm}, -0.14\,\text{m}^{-1})$ with $z = 114\,\text{mm}$, $r_1 = 49\,\text{mm}$, and $K = 0.15$.

from Eq. (6). Thus we expect to find that the period-3 solution of a map with the evolution of iteration will return to its initial value after three iterations. The fixed points of period 3, $\mathbf{Q}^{(3)}$, can be obtained from $\mathbf{F}_K\{\mathbf{F}_K[\mathbf{F}_K[\mathbf{Q}^{(3)}]]\} - \mathbf{Q}^{(3)} = 0$. The variations of period-3 spot size and curvature in a resonator are shown in Fig. 6 with $z = 114\,\text{mm}$, $r_1 = 49\,\text{mm}$, and $K = 0.15$, where the period-3 fixed points are $(w, 1/R) = (0.75\,\text{mm}, 0)$, $(w, 1/R) = (0.64\,\text{mm}, 0.14\,\text{m}^{-1})$, and $(w, 1/R) = 0.64\,\text{mm}, -0.14\,\text{m}^{-1})$. There are two fixed points without matching boundary conditions with $1/R = 0$ at M_1; i.e., the position of the beam waist is not at the output coupler. Besides the period-3 pulse train that can be observed with an oscilloscope, the far-field pattern may contain two other parts. One has a smaller beam size for the solution with its beam waist at M_1; the other is an already divergent spot for the solutions without matching boundary conditions. Similarly, period-4 exists for configurations with $G_1G_2 = (2 \pm \sqrt{2})/4$ for Res $= 1/2$. There are two fixed points that match the curvature of M_1 and two that do not match it. Table 1 summarizes the dynamic behavior for various values of G_1G_2 and z. The character of the nonlinear dynamics depends on the configuration, which is determined by the residue even though the z values are different.

4. SPATIAL–TEMPORAL ANALYSIS OF A KERR-LENS MODE-LOCKED CAVITY

When an ultrashort optical pulse propagates through a Kerr medium, besides causing self-focusing in spatial domain, as discussed above, it will simultaneously undergo self-phase modulation as well as group-velocity dispersion and become broadened. A spatial–temporal analysis involving spatial and temporal *ABCD* matrices was used to transform a Gaussian pulse with a Gaussian spatial profile to optimize the optical pulse with in a KLM laser.[7,8] From the spatial–temporal analogy, the temporal Gaussian pulse can be characterized by the complex pulse parameter

$$\frac{1}{p} = \frac{2\eta}{c} + i\frac{2}{c\sigma^2}, \tag{13}$$

where σ is the pulse width, η is the frequency chirping rate, and c is the speed of light in vacuum. The temporal *ABCD* law transforms the pulse parameter between successive reference planes that have complex pulse parameters p_1 and p_2 through[8]

$$p_2 = \frac{A_t p_1 + B_t}{C_t p_1 + D_t}, \tag{14}$$

where A_t, B_t, C_t, and D_t are the elements of the temporal matrix. A detailed derivation of the temporal *ABCD* matrices for group-velocity dispersion and self-phase modulation of the medium, dispersion compensation of the prism pair, and bandwidth limiting can be found in Ref. 8.

In a numerical simulation, the cavity configuration is the same as that in Fig. 6, and the temporal parameters of the laser are chosen as follows: The Ti:sapphire laser rod has a single-pass group-velocity dispersion of 1280 fs^2; the bandwidth limit is 10 nm, and a pair of the Brewster-angle SF10 prisms with an apex angle of 60.6° is separated by 40 cm. The cavity beam propagates through the apexes of both prisms with insertion of 3 mm. A Gaussian aperture with a diameter of 2 cm is located at mirror M_1. A seeded pulse with initial value $(w_0, R_0, \sigma_0, \eta_0) = (0.7\,\text{mm}, \infty, 1\,\text{ps}, 0)$ propagates along the cavity, and the evolution of spatial parameter $(w, 1/R)$ at M_1 is shown in Fig. 7(a). Note that the total pulse energy remains constant during the propagation; this assumption is appropriate for a Ti:sapphire rod whose gain recovery time is shorter than the round-trip time. The evolution of the spatial parameter in Fig. 7(a) looks like three spirals and jumps among these spirals with regular order. Eventually, it converges to the centers of the spirals. These centers correspond to the period-3 fixed points, which are $(w, 1/R) = q_1(1.46\,\text{mm}, 0.94\,\text{m}^{-1})$, $(w, 1/R) = q_2(1.35\,\text{mm}, -1.04\,\text{m}^{-1})$, $(w, 1/R) = q_3(2.71\,\text{mm}, -0.01\,\text{m}^{-1})$. That is, the evolution eventually becomes steady state, with a sequence q_1–q_2–q_3–q_1–q_2–q_3, etc. Apparently, all the curvatures of fixed points no longer match that of M_1 because the Gaussian aperture (a diffraction loss) that was introduced makes the system dissipative. Because spatial–temporal coupling occurs in the nonlinear medium, the evolution of the pulse width also shows period-3 behavior. Figure 7(b) depicts the dependence of the pulse width on the number of iterations. The pulse width approaches the period-3 solution with $\sigma_1 = 86.72\,\text{fs}$, $\sigma_2 = 80.76\,\text{fs}$, and $\sigma_3 = 110.42\,\text{fs}$. The inset shows an extended plot of the last 10 iterations evolving as a sequence of σ_1–σ_2–σ_3–σ_1–σ_2–σ_3, etc.

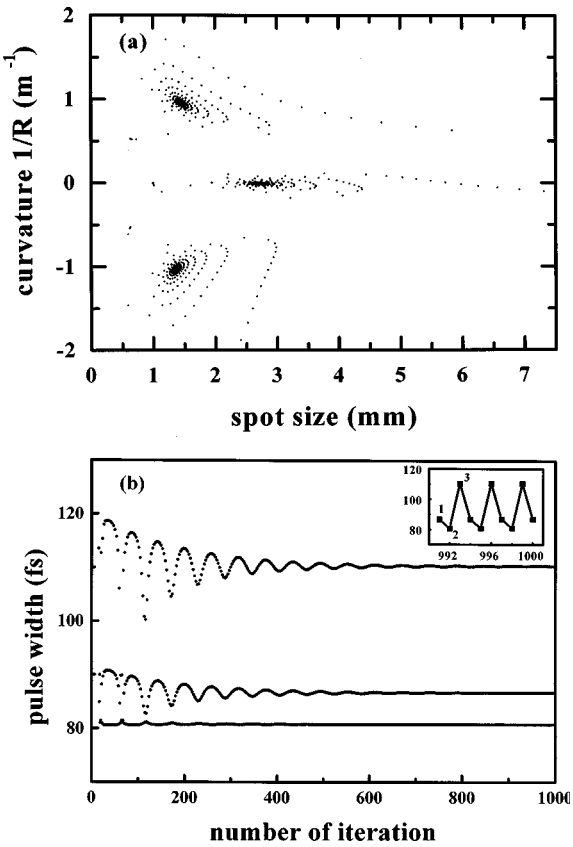

Fig. 7. Spatial and temporal evolutions of period-3. (a) The evolution of the spatial parameter converges to a period-3 steady state, in which the fixed points are $(w, 1/R) = q_1(1.46\,\text{mm}, 0.94\,\text{m}^{-1})$, $(w, 1/R) = q_2(1.35\,\text{mm}, -1.04\,\text{m}^{-1})$, and $(w, 1/R) = q_3(2.71\,\text{mm}, -0.01\,\text{m}^{-1})$. (b) The pulse width also convergently evolves to $\sigma_1 = 86.72$ fs, $\sigma_2 = 80.76$ fs, and $\sigma_3 = 110.42$ fs. Inset, extended plot of the last 10 iterations, the numbers are the subscripts of σ.

Owing to automatic convergence to period-3 in the system, the period-3 solution is more stable than the period-1 solution, even though the period-1 and period-3 steady-state solutions exist simultaneously. We find that the dynamic behavior for which both space and time domains are taken into account is the same as that for which spatial analysis only is considered, because the self-focusing effect governs the characteristics and nonlinear dynamics of the KLM cavity.

Furthermore, we also took into account gain guiding in the spatial domain by introducing a complex matrix of Gaussian duct as

$$\begin{bmatrix} 1 & L \\ -i\dfrac{\lambda g_0}{\pi {w_p}^2} & 1 \end{bmatrix}$$

for most of the pulsed lasers.[26] Here g_0 is the small-signal intensity gain and w_p is the spot size of the pump beam. Because the variation of the pumping spot size in the gain medium is small, e.g., ~1% variation for a 100-μm beam waist through a 2-cm medium, we assume that w_p is constant and simply add a gain-guiding matrix at the center of Kerr medium. The result is the same as the previous one, i.e., that the system eventually converges to period-3, and only the former convergent rate (with a gain-guiding effect) is faster than the latter one.

5. IRREGULAR BEHAVIOR

In this section we show that, with the same configuration as in Fig. 6 in which the transition from period-1 to period-3 occurs as K approaches 0.08354, the system exhibits complicated dynamic behavior as the Kerr parameter increases. The intensity fluctuation versus number of measurements is shown in Fig. 8 with $K = 0.4$. To observe the long-term evolution, we obtain each measurement of the intensity variation by averaging over 300 iterations and then normalizing the result to the average intensity over all data points. The regular evolution appears as line (b) in Fig. 8 with the initial value $(w_0, 1/R) = (0.705\,\text{mm}, 0)$. Such an evolution corresponds to the regular orbit shown as the invariant circle in a conservative map.[23] When the initial spot size varies to $w_0 = 0.71$ mm, the evolution becomes irregular, as shown in curve (a) of Fig. 8. This behavior results from the fact that the nonlinear perturbation brings about the breakdown of the separatix accompanied by creation of a stochastic layer. These initial-condition-dependent irregular behaviors are examples of classic chaos.[23] In fact, the complicated dynamics in this configuration can be predicted from the residue theorem that a system with Res = 3/4 is typically unstable. However, when Gaussian loss or gain guiding is considered, the irregular behavior gradually decays to period-3 because its long-term behavior is governed by the damping effect. If the averaged time period relative to a sudden perturbation, such as a small variation of the Kerr effect, the thermal effect, or other noise, is shorter than the aforementioned decay rate, the irregular evolution may be continuously excited before it is damped down to period-3. In this case, we believe that an irregular pulse train will also be observed at a configuration near the period-3 configuration.

6. DISCUSSION

We have shown above that the nonlinear dynamics of fundamental beam propagation depends on the cavity con-

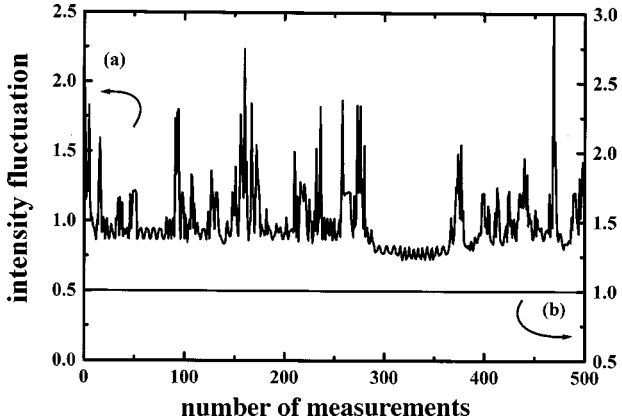

Fig. 8. Evolution of the intensity fluctuation. The intensity fluctuation is normalized to the average intensity in this figure. The initial values are (a) $w_0 = 0.71$ mm and (b) $w_0 = 0.705$ mm, with $z = 114$ mm, $x = 49$ mm, and $K = 0.4$.

figuration in a KLM cavity. The reader may what the difference is between our results and the similar subharmonic oscillations already explained well by total mode locking.[9,10] Total mode locking is the phase locking of the longitudinal modes and the high-order transverse modes that leads to spatial sweeping of the beam with a frequency given by the spacing between the transverse modes. It is a result of the linear superposition of cavity eigenmodes with a definite phase shift and belongs to spatial dynamics,[9] but the irregular behavior that originates from nonlinear dynamics cannot be directly expressed in terms of linear superposition. In contrast, the dynamics in our approach is based on propagation of the fundamental mode through nonlinearly modifying the spatial beam profile to manifest an intensity variation in the time domain. One can directly determine the route of this dynamics from period-1 to irregular behavior by increasing nonlinear parameter K. Therefore these two approaches represent two different classes of nonlinear dynamic behavior.

Although these two approaches show the dependence of cavity configuration on nonlinear dynamics, the predicted configurations for subharmonic oscillations are somewhat different. Based on total mode locking, one will observe period-2, period-3, or period-4 for the configurations that have ratios of 2, 3, or 4, respectively, of longitudinal mode spacing ω_L to transverse mode spacing Ω. Because the transverse mode spacing[15] is $\Omega = (\omega_L/\pi)\cos^{-1}(\sqrt{G_1G_2})$, period-2, period-3, and period-4 will occur at $G_1G_2 = 0,1/4,1/2$, respectively. However, from our approach, period-2, period-3, and period-4 will occur at $G_1G_2 = 1/2,1/4$ (or 3/4), $(2 \pm \sqrt{2})/4$, respectively. Through the aforementioned difference, we propose that an experiment to observe the dynamic behavior for the corresponding configurations will help to distinguish these two classes of nonlinear dynamics. Furthermore, inasmuch as the Hermite–Gaussian modes are identical to the wave functions of a quantum-mechanical harmonic oscillator and the Hamiltonian associated with our map is a form of simple harmonic oscillation, [18] this may be the reason for the similarity of the results derived from these two approaches.

7. CONCLUSION

In summary, we have shown that typical nonlinear dynamics depends on the cavity configuration. From analyzing the iterative map of a general cavity by Greene's residue theorem, we found that the nonlinearly sensitive configurations correspond to the product of generalized G parameters equal to 1/2, 1/4 (or 3/4), and $(2 \pm \sqrt{2})/4$. It is interesting to note that these configurations are located within the geometrically stable region. This result implies that the nonlinear effects may break the stability of these self-consistent Gaussian modes derived from linear cold cavities.

When the fundamental Gaussian beam propagates in a KLM cavity, nonlinear dynamics intrinsically exists in the KLM cavity because the Kerr effect will result in mode locking and induce nonlinearly dynamic behavior simultaneously. The numerical results confirm that period doubling, tripling, and quadrupling can be obtained at the aforementioned configurations. Besides the existence of multiple-period behavior in a nonlinear KLM cavity, we have found that irregular evolution occurs when the nonlinear effect is increased.

These specific configurations that are sensitive to the nonlinear effects are based on analyzing a generalized cavity. This research gives a useful suggestion for laser cavity design for studying the nonlinear phenomena of Gaussian modes.

ACKNOWLEDGMENT

This research was partially supported by the National Science Council of the Republic of China under grant NSC89-2112-M-009-026.

W.-F. Hsieh's e-mail address is wfhsieh@cc.nctu.edu.tw.

REFERENCES

1. D. E. Spence, P. N. Kean, and W. Sibbett, "60-fs pulse generation from a self-mode-locked Ti:sapphire laser," Opt. Lett. **16**, 42–44 (1991).
2. M. Piche, "Beam reshaping and self-mode-locking in nonlinear laser resonators," Opt. Commun. **86**, 156–160 (1991).
3. G. W. Pearson, C. Radzewicz, and J. S. Krasinski, "Analysis of self-focusing mode-locking lasers with additional highly nonlinear self-focusing elements," Opt. Commun. **94**, 221–226 (1992).
4. J. Herrmann, "Theory of Kerr-lens mode locking: role of self-focusing and radially varying gain," J. Opt. Soc. Am. B **11**, 498–512 (1994).
5. G. Cerullo, S. De Silvestri, V. Magni, and L. Pallaro, "Resonators for Kerr-lens mode-locked femtosecond Ti:sapphire lasers," Opt. Lett. **19**, 807–809 (1994).
6. K.-H. Lin and W.-F. Hsieh, "An analytical design of asymmetrical Kerr lens mode-locking laser cavities," J. Opt. Soc. Am. B **11**, 737–741 (1994).
7. J. L. A. Chilla and O. E. Martinez, "Spatial-temporal analysis of the self-mode-locked Ti:sapphire laser," J. Opt. Soc. Am. B **10**, 638–643 (1993).
8. K.-H. Lin and W.-F. Hsieh, "Analytical spatio-temporal design of Kerr lens mode-locked laser resonators," J. Opt. Soc. Am. B **13**, 1786–1793 (1996).
9. D. Cote and H. M. van Driel, "Period doubling of a femtosecond Ti:sapphire laser by total mode locking," Opt. Lett. **23**, 715–717 (1998).
10. S. R. Bolton, R. A. Jenks, C. N. Elkinton, and G. Sucha, "Pulse-resolved measurements of subharmonic oscillations in a Kerr-lens mode-locked Ti:sapphire laser," J. Opt. Soc. Am. B **16**, 339–344 (1999).
11. V. L. Kalashnikov, I. G. Poloyko, and V. P. Mikhailov, "Regular, quasi-periodic, and chaotic behavior in continuous-wave solid-state Kerr-lens mode-locked lasers," J. Opt. Soc. Am. B **14**, 2691–2695 (1997).
12. Q. Xing, L. Chai, W. Zhang, and C. Wang, "Regular, period-doubling, quasi-periodic, and chaotic behavior in a self-mode-locked Ti:sapphire laser," Opt. Commun. **162**, 71–74 (1999).
13. M.-D. Wei, W.-F. Hsieh, and C. C. Sung, "Dynamics of an optical resonator determined by its iterative map of beam parameters," Opt. Commun. **146**, 201–207 (1998).
14. J. M. Greene, "A method for determining a stochastic transition," J. Math. Phys. **20**, 1183–1201 (1979).
15. A. E. Seigman, *Lasers* (University Science, Mill Valley, Calif., 1986), Chaps. 20 and 21.
16. H. Kogelnik, "Imaging of optical modes—resonators with internal lenses," Bell Syst. Tech. J. **44**, 455–494 (1965); H.

Kogelnik and T. Li, "Laser beams and resonators," Appl. Opt. **5**, 1550–1556 (1966).
17. H. A. Haus, J. G. Fujimoto, and E. P. Ippen, "Analytic theory of additive pulse and Kerr lens mode-locking," IEEE J. Quantum Electron. **28**, 2086–2096 (1992).
18. M.-D. Wei, W.-F. Hsieh, and C. C. Sung, "The preferable resonators for Kerr-lens mode-locking determined by stability factors of their iterative maps," Opt. Commun. **155**, 406–412 (1998).
19. L. M. Sanchez and A. A. Hnilo, "Optical cavities as iterative maps in the complex plane," Opt. Commun. **166**, 229–238 (1999).
20. K.-H. Lin, Y. Lai, and W.-F. Hsieh, "Simple analytic method of cavity design for astigmatism compensated Kerr lens mode-locked ring lasers and its application," J. Opt. Soc. Am. B **12**, 468–475 (1995).
21. M. Mechendale, T. R. Nelson, F. G. Omenetto, and W. A. Schroeder, "Thermal effects in laser pumped Kerr-lens modelocked Ti:sapphire lasers," Opt. Commun. **136**, 150–159 (1997).
22. B. E. Lemoff and C. P. J. Barty, "Generation of high-peak-power 20 fs pulses from a regeneratively initiated, self-mode-locked Ti:sapphire laser," Opt. Lett. **17**, 1367–1369 (1992).
23. R. S. MacKay, *Renormalisation in Area-Preserving Maps* (World Scientific, Singapore, 1993), Chap. 1.
24. A. J. Lichtenberg and M. A. Lieberman, *Regular and Chaotic Dynamics* (Springer-Verlag, New York, 1992), Chap. 3.
25. J.-M. Shieh, F. Ganikhanov, K.-H. Lin, W.-F. Hsieh, and C.-L. Pan, "Completely self-starting picosecond and femtosecond Kerr-lens mode-locked Ti:sapphire laser," J. Opt. Soc. Am. B **12**, 945–949 (1995).
26. F. Salin and J. Squier, "Gain guiding in solid-state lasers," Opt. Lett. **17**, 1352–1354 (1992).